Annals of Nuclear Energy 124 (2019) 187–197

Contents lists available at ScienceDirect

Annals of Nuclear Energy

journal homepage: www.elsevier.com/locate/anucene

# Development and verification of a model for generation of MSFR few-group homogenized cross-sections based on a Monte Carlo code OpenMC

Kun Zhuang [a,*], Xiaobin Tang [a], Liangzhi Cao [b]

[a] College of Material Science and Technology, Nanjing University of Aeronautics and Astronautics, Nanjing, JiangSu 211106, PR China
[b] School of Nuclear Science and Technology, Xi'an Jiaotong University, Xi'an, ShannXi 710049, PR China

ARTICLE INFO

*Article history:*
Received 3 August 2018
Received in revised form 13 September 2018
Accepted 29 September 2018

*Keywords:*
MSFR
Few-group parameter
Homogenization
OpenMC
Neutronics

ABSTRACT

A concept of molten salt fast reactor (MSFR) was proposed in EVOL to burn transuranium element discharged from pressurized water reactors. MSFR is featured by fast spectrum and using liquid fuel salt containing $UF_4$ or $ThF_4$. Some issues are presented, for instance, global material arrangement affects the local neutron spectrum due to long neutron free path, and fluoride salt (LiF-$BeF_2$) has nonnegligible thermal neutron scattering effect. Thus, lattice code prepared for thermal-spectrum reactor is not suitable for MSFR calculation. In this study, "two-step" calculation scheme combining Monte Carlo method and deterministic method was prepared for MSFR calculation. A tool named TRANS was developed to transfer tally data from an open source Monte Carlo code OpenMC into few-group homogenized cross-sections, and one benchmark based on pressurized water reactor and two types of model based on MSFR were used for verification. Besides, the applicability of few-group parameters generated by different model to MSFR whole-core calculation was analyzed. Finally, MSFR neutronics characteristics at steady-state were calculated using MOREL. The results show that the few-group parameters generated by one-dimension (1D) and two-dimension (2D) model are correct, and it is feasible to use OpenMC to generate few-group parameters. In case of 1D homogenization model, few-group parameters by 1D model (b) can give more accurate results both for eigenvalue and flux distribution. In MSFR whole-core calculation, using few-group cross-sections generated by 2D model has better accuracy in flux distribution, however, using few-group cross-sections generated by 1D model has better accuracy in $k_{eff}$ calculation. Moreover, the neutronics parameters of MSFR calculated by MOREL code agree well with that by other institutes.


## 1. Introduction

Molten salt reactor (MSR) with the fuel dissolved into the liquid salt has been identified as one of the six Generation-IV reactor types in the Generation-IV International Forum (GIF-IV) due to its excellent advantages in terms of sustainability, non-proliferation, safety and waste management (Pioro, 2016). The history of MSR research dates back to 1950s-1980s, when the program of Aircraft Experiment (ARE) (Bettis et al., 1957), Molten Salt Reactor Experiment (MSRE) (Haubenreich, 1969) and the concept of Molten Salt Breeder Reactor (MSBR) (Rosenthal et al., 1972) were developed by Oak Ridge National Laboratory (ORNL). The feature of using liquid fuel in MSR system provides large flexibility in aspect of reactor design and fuel recycling scheme. Historically, thermal-spectrum MSBR with graphite moderator was proposed to breed fissile isotopes based on Th-U fuel cycle. Nowadays, fast-spectrum MSRs as an actinide burning reactor or breeder reactor interest researchers due to the global shortage of uranium resources and the increase of nuclear waste. The energy-dependent effective fission neutron number of fissile nuclide in fast energy region is greater than that in thermal energy region (Yang, 2012), thus, fast-spectrum MSR has more excellent breeding performance. A concept of Molten Salt Fast Reactor (MSFR) was proposed in EVOL (Evaluation and Viability of Liquid Fuel Fast Reactor System) to burn transuranium element (TRU) discharged from pressurized water reactors (PWRs) (Allibert et al., 2016; Fiorina et al., 2014). The primary feature of the MSFR concept versus that of other older MSR designs is the removal of the moderator and other structures from the active core (moderator-free core), which makes it possible to breed U233 based on fast neutron spectrum and thorium fuel cycle. Due to a unique potential (excellent

* Corresponding author at: 29 Jiangjun Avenue, Nanjing 211106, PR China.
*E-mail address:* kzhuang@nuaa.edu.cn (K. Zhuang).

https://doi.org/10.1016/j.anucene.2018.09.037
0306-4549/

safety coefficients, smaller fissile inventory, no need for criticality reserve, simplified fuel cycle etc.), the MSFR has been recognized as a long-term alternative to solid fueled fast neutron systems by the Generation IV International Forum as of 2008 (Serp et al., 2014).

In comparison with traditional solid-fuel reactor and graphite-moderator MSR, MSFR has some special characteristics due to the fact that the liquid fuel salt containing $UF_4$ or $ThF_4$ circulates through primary loop and moderator-free core leads to fast-spectrum. Firstly, MSFR has long neutron free path, weak local resonance self-shielding effect and strong global neutron spectrum coupling (Zhou, 2017). Thus, homogenization method considering global material arrangements need to be developed. Secondly, MSFR generally adopts fluoride salt (LiF-$BeF_2$) as carrier salt, which has nonnegligible thermal neutron scattering effect (Li et al., 2016). However, some lattice codes for PWR lack related thermal scattering data, and it would bring error if those codes are used for MSFR homogenization calculation. Thirdly, the delayed neutron precursors (DNPs) continuously change their position along with fuel circulation and decay in external loop, and the core multiplication factor is dependent on the fuel velocity field. Fourthly, the fact that the fuel is dissolved in the coolant rather than separated from the coolant by the claddings results in a much stronger coupling phenomenon between the neutronics and thermal-hydraulics.

Lot of efforts have been made to study MSR neutronics and thermal-hydraulics characteristics based on different methods and simplifications. Those methods are generally divided into two categories: direct method and "two-step" method.

The direct method refers to a method of directly using the original nuclear data for core calculation, usually with less assumptions. Monte Carlo method is the most common direct method. Heuer et al. and Nuttin et al. employed a Monte Carlo code MCNP (Briesmeister, 1997) and a home-made materials evolution code REM to study MSFR fuel cycle characteristics (Heuer et al., 2014; Nuttin et al., 2005). Aufiero extended the applicability of Monte Carlo code SERPENT (Leppänen et al., 2015) for MSFR effective delayed neutron fraction calculation based on one-group approximation (Aufiero et al., 2014). The MSFR study in The Kurchatov Institute was performed by coupling MCNP-4B and the ORIGEN2.1 code (Brovchenko and Merle-Lucotte, 2013). Aufiero et al. extended SERPENT-2 code for burn-up calculations by taking into account online fuel reprocessing (Aufiero et al., 2013). "Two-step" method is a classical method for core neutronics calculation. Fiorina et al. adopted ECCO cell code to generate few-group cross-sections, then investigated the MSFR core physics and fuel cycle characteristics with ERANOS code (Fiorina et al., 2013). Zhang et al. and Wang and Cao et al. developed MSR code by using DRAGON or HELIOS code for two-group homogenization calculation (Wang and Cao, 2016; Zhang et al., 2009). Linden employed SCALE6 to obtain cross-sections of nine energy groups based on one-dimension (1D) geometry model (Linden, 2012). Frima used 1D transport code XSDRNPM to generate few-group cross-sections based on an equivalent two-dimensional model considering MSFR radial and axial material arrangement (Frima, 2013). In Helmholtz-Zentrum Dresden-Rossendorf, HELIOS 1.10 code system with the internal 47 energy group library was used for MSFR simulations (Rachamin et al., 2013). Fridman et al. generated three-group cross-sections of the core and blanket region using SERPENT code, then performed whole-core deterministic calculations (Fridman and Leppänen, 2011; Tuominen, 2015). Some researchers developed the fuel cycle analysis procedures for MSRs based on SCALE/TRITON (Powers et al., 2013; Sheu et al., 2013; Yu et al., 2017). Zhou et al. and Hu et al. used Monte Carlo code OpenMC (Romano et al., 2015) to generate multi-group cross-sections, but without verification of homogenization geometry model and few-group cross-sections (Hu et al., 2017; Zhou et al., 2018).

Some deficiencies are found in above mentioned MSFR studies. Firstly, even though the Monte Carlo method is flexible for reactor with complex geometry and neutron spectrum, it still spends a lot of computational time in whole-core simulations. And "two-step" calculation scheme shows an advantage in terms of computational time. Secondly, DRAGON and HELIOS codes are usually used for analysis of thermal-spectrum reactors, and a typical thermal spectrum is used for the weighting of their multi-group master libraries. The applicability of those multigroup nuclear data libraries for MSFR has not been demonstrated so far. Thirdly, in MSFR, local neutron spectrum will be affected by global material arrangements due to long neutron free path, and the few-group cross-sections may differ as a function of space, even within the same material. Therefore, it is necessary to develop homogenization model considering global material arrangement for MSFR calculations. Besides, most researchers lack detailed verifications of the accuracy of few-group cross-sections. Fourthly, Monte Carlo code SERPENT is a good choice to generate few-group homogenized cross-sections, however, SERPENT code is only accessed by member institutes.

This study aims to develop a method and model for generating few-group homogenized cross-sections for MSFR whole-core calculation, and to verify comprehensively few-group cross-sections. Considering the advantages of Monte Carlo method and deterministic method, arbitrary energy group structure definition and geometric flexibility for the former and excellent computational efficiency for the latter (Leppänen et al., 2015; Li, 2012; Romano et al., 2015; Wang et al., 2010), "two-step" calculation scheme combining Monte Carlo method and deterministic method was prepared for MSFR calculation. An open source Monte Carlo code OpenMC (Romano et al., 2015) developed by Computational Reactor Physics Group at Massachusetts Institute of Technology (MIT) was used to generate few-group homogenized cross-sections. However, OpenMC can't directly output few-group parameters, thus, a tool named TRANS was developed to transfer tally data of OpenMC into few-group parameters and the method is described in Section 2.1. Furthermore, one benchmark based on PWR, and 1D and two-dimension (2D) models based on the MSFR core configuration were employed to verify the process of generating few-group cross-sections. 1D model only considers radial material arrangement and 2D model represents actual 2D R-Z MSFR system. Then, few-group cross-sections produced by 1D and 2D model were respectively employed in MSFR whole-core calculation, and OpenMC results serve as reference. The neutron flux distribution using few-group parameters generated by 2D model show a better agreement with reference compared with that using few-group parameters generated by 1D model. Finally, a MSR analysis code MOREL (Zhuang et al., 2015) developed in our previous study was performed to calculate the temperature coefficients and effective delayed neutron fraction based on few-group parameters generated by 2D model. To prevent confusion, in the full text, 'steady state' indicates system/core reaches a steady state, however, 'static condition' and 'flow condition' represent fuel salt motion state.

## 2. Methodology and numerical method

The overview flowchart of generating few-group cross-sections based on OpenMC code is depicted in Fig. 1: 1) temperature-dependent continuous-energy neutron data library in ACE format is produced by NJOY code based on ENDF/B-VII.1 library (MacFarlane and Muir, 1994); 2) Reaction rates of different reaction types and neutron flux are tallied in OpenMC calculation; 3) An in-house development tool TRANS is used to transfer tally data into few-group cross-sections for the following whole-core calculations.

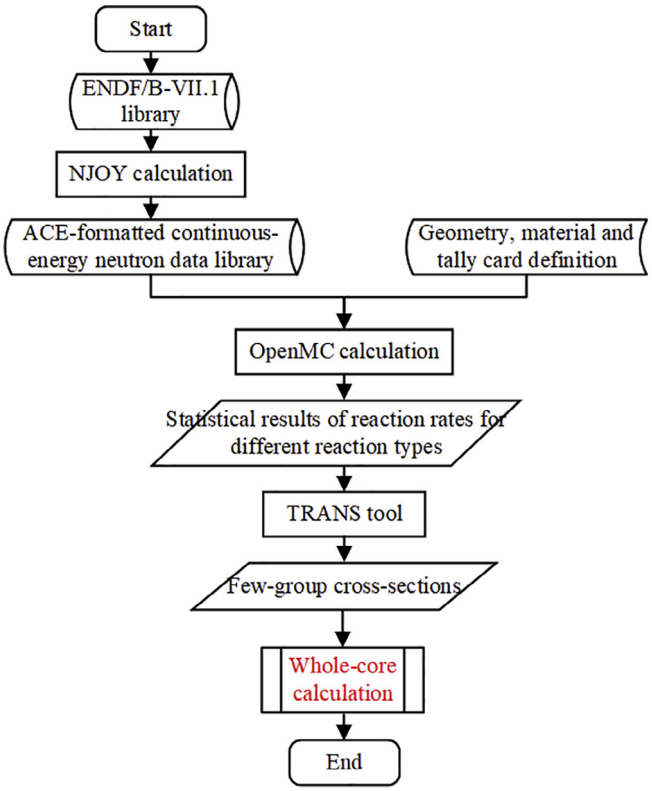


**Fig. 1.** The flowchart of generating few-group cross-sections based on OpenMC code.

### 2.1. Few-group cross-sections generation

In MSFR system, the special features (such as fast neutron spectrum and nonnegligible thermal scattering effect of fluoride salt) lead some lattice codes prepared for thermal-spectrum reactor not to be applicable for generation of few-group homogenized cross-sections. In order to adapt for the flexibility of neutron spectrum and geometry, an open source Monte Carlo code OpenMC developed by MIT was employed to generate few-group cross-sections. Before OpenMC calculation, continuous-energy neutron data library in ACE format and thermal $S(\alpha,\beta)$ cross-sections at given temperature are generated using NJOY code based on ENDF/B-VII.1. The data at user-defined energy group structure in terms of flux, fission reaction rate, scattering reaction rate, and absorption reaction rate were tallied by OpenMC. An in-house development code TRANS was used to transfer those tally results into few-group parameters based on the Eqs. (1), (2) and (3). 6 groups of delayed neutron precursors were employed in this study.

$$\Sigma_{x,g} = \frac{R_{x,g}}{\phi_g} \tag{1}$$

$$\beta_i = \frac{\beta_i \sum_{g=1}^{G} \nu\Sigma_{f,g}\phi_g}{\sum_{g=1}^{G} \nu\Sigma_{f,g}\phi_g} \tag{2}$$

$$\lambda_i = \frac{\lambda_i \beta_i \sum_{g=1}^{G} \nu\Sigma_{f,g}\phi_g}{\beta_i \sum_{g=1}^{G} \nu\Sigma_{f,g}\phi_g} \tag{3}$$

where $x$ indicates neutron reaction type; $g$ represents energy group; $R$ is neutron reaction rate and can be obtained by defining such as <absorption>, <nu-fission>, et al. in OpenMC tally card; neutron scalar flux $\phi$ is total flux in the area of interest and can be obtained by defining <flux> in OpenMC tally card; $\Sigma$is macroscopic cross-section; $\beta_i$ and $\lambda_i$ are respectively DNP fraction and decay constant; $i$ is DNP group number; $\nu\Sigma_{f,g}$ means neutron production cross-section; $\beta_i\sum_{g=1}^{G}\nu\Sigma_{f,g}\phi_g$ and $\sum_{g=1}^{G}\nu\Sigma_{f,g}\phi_g$can be obtained by defining respectively <delayed-nu-fission> and <nu-fission> in OpenMC tally card; $\lambda_i\beta_i\sum_{g=1}^{G}\nu\Sigma_{f,g}\phi_g$ can be obtained by defining <tracklength> in OpenMC tally card.

Due to large statistical uncertainty and poor efficiency in tallying higher order scattering moment matrix, the anisotropic scattering cross-section is only considered to the first order scattering moment matrix. And the zeroth order self-scattering moment matrix and total cross-section are corrected by the transport correction as shown in Eqs. (4) and (5), respectively. In addition, diffusion coefficient $D_g$ is defined as Eq. (6). The uncertainty of few-group homogenized cross-section depends on statistical uncertainty of neutron flux, which can reach to be around 1.0E-5 with enough simulation neutron particles.

$$\Sigma'_{s,g\to g} = \Sigma_{s,g\to g} - \sum_{g'=1}^{G} \Sigma_{s1,g'\to g} \tag{4}$$

$$\Sigma'_{t,g} = \Sigma_{t,g} - \sum_{g'=1}^{G} \Sigma_{s1,g'\to g} \tag{5}$$

$$D_g = \frac{1}{3\Sigma'_{t,g}} \tag{6}$$

where $g$ represents energy group; $\Sigma_{s1}$ represents first order scattering moment matrix; $\Sigma_s$ is zeroth order self-scattering moment matrix; $\Sigma'_s$ is scattering moment matrix with transport correction; $\Sigma_t$ is the total cross-section and $\Sigma'_t$ is total cross-section with transport correction; $D$is diffusion coefficient.

### 2.2. Neutronics model for MSFR calculation

The release of the delayed neutron is not in the same location as the event of fission reaction since DNPs flow with liquid fuel salt in primary loop during MSFR operation. The effect of flowing fuel on the prompt neutron is not considered. In this study, the traditional 3D neutron diffusion equations were extended for MSR analysis by introducing a convection term into DNPs balance equation, as shown in Eqs. (7) and (8).

$$-\nabla\cdot D_g(r)\nabla\phi_g(r) + \Sigma_{t,g}(r)\phi_g(r) = S'_g(r) \quad g = 1,2,...,G \tag{7}$$

$$Q(r) - \lambda_i C_i(r) - \nabla[\boldsymbol{U}C_i(r)] = 0 \quad \mathrm{i} = 1,2,...,\mathrm{I} \tag{8}$$

where $\phi$ is scalar flux; $r$ is spatial position; $C$ is DNP concentration; $\boldsymbol{U}$ represents fuel velocity vector;$\lambda$ is decay constant of precursors; $D$ and $\Sigma_t$ are respectively diffusion coefficient and total cross-section; $G$ and $I$ are the total number of energy group and DNP families, respectively; $S'_g$ and $Q(r)$ are defined as:

$$S'_g(r) = \sum_{g'=1}^{G}\Sigma_{g'g}(r)\phi_{g'}(r) + \frac{1}{k_{eff}^{s}}(1-\beta)\chi_{pg}\sum_{g'=1}^{G}\nu\Sigma_{fg'}(r)\phi_{g'}(r) + \sum_{i=1}^{I}\chi_{dgi}\lambda_i C_i(r) \quad \mathrm{i} = 1,2,...,\mathrm{I} \tag{9}$$

$$Q(r) = \frac{1}{k_{eff}^{s}}\sum_{g'=1}^{G}\beta_i\nu\Sigma_{fg'}(r)\phi_{g'}(r) \tag{10}$$

where standard notations in neutronics are used and $k_{eff}^{s}$ indicates effective multiplication factor at steady-state; $\beta_i$ and $\lambda_i$ are DNP fission fraction and decay constant, respectively. $\chi_{pg}$ is prompt neutron fission spectrum and $\chi_{dgi}$ is delayed neutron fission spec-

trum for *i*-th DNP group; Subscripts of 'p' and 'd' represent prompt and delayed neutron; Other notations have the same meaning with that in Eqs. (7) and (8).

A 3D MSR analysis code MOREL was performed for whole-core calculation. Prompt neutron Equation was solved by analytic basis functions expansion method (ABFEN) (Wang et al., 2010; Zhuang et al., 2015), and the solving method of DNP Equation will be presented in the following section. Equation and Equation are coupled with each other by source term during fission source iteration, and the effective multiplication factor is updated as the following expression (Zhuang et al., 2017):

$$k_{eff}^{s}=\frac{\int_V\sum_{g=1}^{G}(1-\beta)\chi_{pg}\sum_{g'=1}^{G}\nu\Sigma_{fg'}(r)\phi_{g'}^{n}(r)dr+\int_V\sum_{g=1}^{G}\left(\sum_{i=1}^{I}\chi_{dgi}\lambda_i C_i^{n}(r,t)\right)dr}{\frac{1}{k_{eff}^{s,n-1}}\left(\int_V\sum_{g=1}^{G}(1-\beta)\chi_{pg}\sum_{g'=1}^{G}\nu\Sigma_{fg'}(r)\phi_{g'}^{n-1}(r)dr+\int_V\sum_{g=1}^{G}\left(\sum_{i=1}^{I}\chi_{dgi}\lambda_i C_i^{n-1}(r,t)\right)dr\right)} \tag{11}$$

where standard notations in neutronics are used; $n$ represents the number of fission source iteration; $V$ indicates the volume of whole system; Other notations have the same meaning with that in Eqs. (7-10).

### 2.3. Delayed neutron precursors drift

In this study, the DNP drift only considers axial velocity field of fuel salt. The velocity vector $\boldsymbol{U}$ is written as $u(x,y,z)\vec{e}_x + v(x,y,z)\vec{e}_y + w(x,y,z)\vec{e}_z$, where $u(x,y,z)$, $v(x,y,z)$ and $w(x,y,z)$ are respectively the components of the flow velocity along the $x$, $y$, and $z$ directions at the position $(x,y,z)$. Equation (8) is reduced to Eq. (12) with omitting DNP family index $i$.

$$\frac{\partial[w(x,y,z)C(x,y,z)]}{\partial z}+\lambda C(x,y,z)=Q(x,y,z) \tag{12}$$

where $(x,y,z)$ represents spatial position $r$; $Q(x,y,z)$ is DNP source at position $(x,y,z)$, and standard notations in neutronics are used for other notations.

ABFEN method was employed to solve Eq. (7). The expansion of neutron flux $\phi(x,y,z)$ in one nodal and $k_{eff}^{s}$ were obtained during fission source iterations. Thus, as described in Eq. (13), the DNP source in form of second-order polynomial will be calculated by integrating $Q(x,y,z)$ shown in Eq. (10) along x-y direction. In addition, $Q$ is just a function of z in one nodal.

$$Q(x,y,z)=a_0(x,y,z)+a_1(x,y,z)z+a_2(x,y,z)z^2 \tag{13}$$

where $a_0$, $a_1$ and $a_2$ are the coefficients.

The DNP concentration is analytically obtained from Equation with known DNP source, and is described as following:

$$C(x,y,z)=\frac{1}{w(x,y,z)}\left[\int_0^z Q(x,y,z')e^{\int_0^{z'}\frac{\lambda(x,y,z'')}{w(x,y,z'')}dz''}dz' +w(x,y,0)C(x,y,0)\right]e^{-\int_0^z\frac{\lambda(x,y,z')}{w(x,y,z')}dz'} \tag{14}$$

where $w(x,y,z)$ is axial velocity of fuel salt at position $(x,y,z)$, and standard notations in neutronics are used.

In MSR system, DNPs drift along with circulation of fuel salt in whole primary loop. As a result, part of DNPs decay outside of the core, and the un-decayed ones will reenter reactor core. Thus, the DNP concentration at inlet and outlet boundary satisfy:

$$\iint_{A_{in}} w(x,y,0)C(x,y,0)dA=\iint_{A_{out}} w(x,y,H)C(x,y,H)dA\cdot exp(-\lambda\cdot\tau) \tag{15}$$

where $C$ is DNP concentration; $\lambda$ is decay constant of DNP;$A_{in}$ and $A_{out}$are inlet and outlet core flow area, respectively; $\tau$is the time of fuel salt spent flowing through external loop.

## 3. Numerical results

A reference configuration of the MSFR proposed in EVOL project was adopted for analysis, as depicted in Fig. 2 (Merle-Lucotte et al., 2011). The MSFR concept is a 3000 MWth fast-spectrum MSR based on $^{233}U/^{232}Th$ fuel cycle, and the inlet and outlet fuel temperature in the core are 923 K and 1023 K, respectively. Two kinds of initial fuel compositions are employed in this simulation. Both are made up of a LiF-$ThF_4$-$(HN)F_4$ mixture, but the heavy nuclides composition differs. One adopts $^{233}U$ (U233-started) as fission material and the other one uses TRU (TRU-started) coming from 60 GWd/ton waste from a PWR with plutonium as the main element. As shown in Fig. 2, the inner cylinder core filled with fuel salt is surrounded by the fertile blanket to improve the global breeding performance. The fertile blanket, filled with a fertile salt LiF-ThF4 with 22.5% of $^{232}Th$, is surrounded by $B_4C$ reflector that absorbs the leaking neutrons and protects the heat exchanges. The fuel salt spends 4 s flowing through the primary circuit. More detailed descriptions can be referred to (Frima, 2013; Merle-Lucotte et al., 2011). In this study, the fuel salt reprocessing scheme and thermal-hydraulics feedback were not considered.

### 3.1. Verification of few-group homogenized cross-sections

To verify the method of few-group homogenized cross-sections generated by OpenMC code, a benchmark of 2D 3 × 3 assembly at hot-zero-power (HZP) and beginning-of-cycle (BOC) based on Watts Bar Nuclear Plant Unit 1 (WBN1) reactor (Godfrey, 2014), and 1D model and 2D model based on MSFR core configuration depicted in Fig. 2 were employed. 1D model only considers MSFR radial material arrangement and 2D model represents actual 2D R-Z MSFR system. Since many researchers employed 1D homogenization model for generation of few-group parameters, the comparison between 1D model and 2D model in this study is to verify which one model produces more accurate few-group cross-sections. In addition, the effect of that fertile salt and its surrounding structure material Ni-based alloy are homogenized into one homogenized material was analyzed. Due to the approximations adopted in Fick's law, a natural difference appears between diffusion theory and transport theory. In order to eliminate this difference, a transport code DNTR was employed instead of direct use of MOREL in the following verifications since Monte Carlo results serve as reference. DNTR is based on nodal SN transport method for three-dimensional triangular-z geometry and has been verified in previous study (Lu and Wu, 2007). The triangle nodes used in DNTR are generated by ANSYS-14.0 in this study.

#### 3.1.1. Benchmark of 2D WBN1 3 × 3 assembly at HZP and BOC

This problem is a 2D slice from the midplane of the center nine assemblies in the WBN1 startup core, and the fuel is at BOC and HZP isothermal conditions. Three cases named WBN1-3A (no control rod), WBN1-3B (24 Ag-In-Cr control rods) and WBN1-3C (24 $B_4C$ control rods) were adopted. As the loading pattern for this

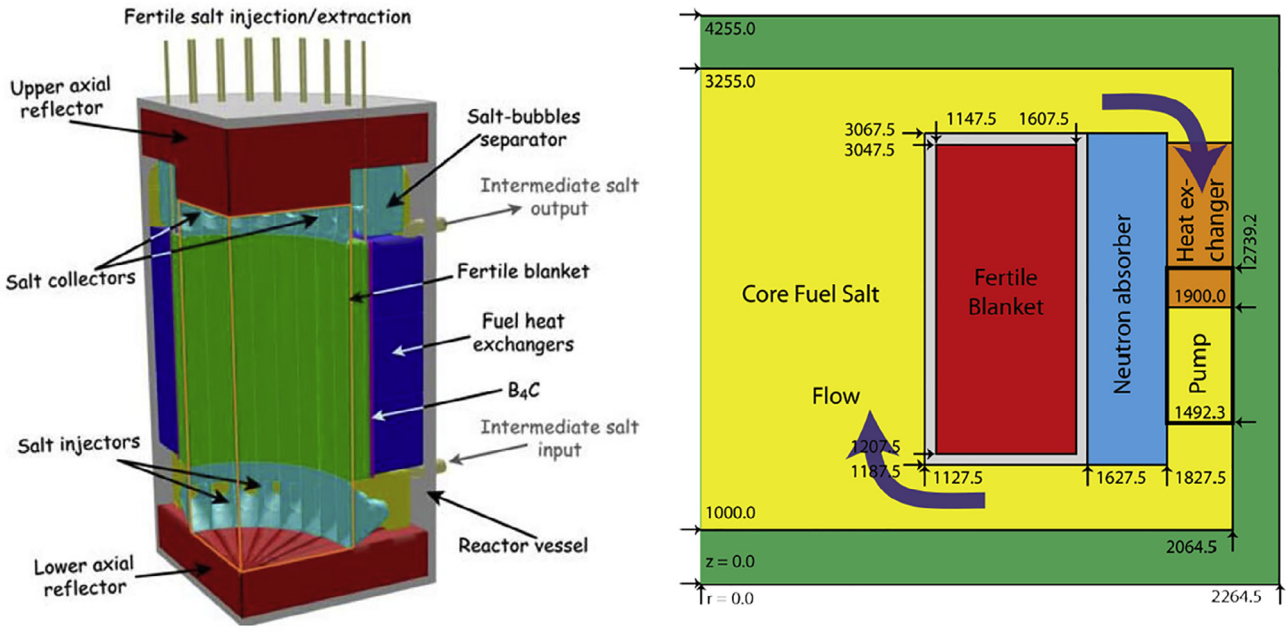


**Fig. 2.** 3D view of a quarter of MSFR reactor core (left) and corresponding parameters (right) (Merle-Lucotte et al., 2011).

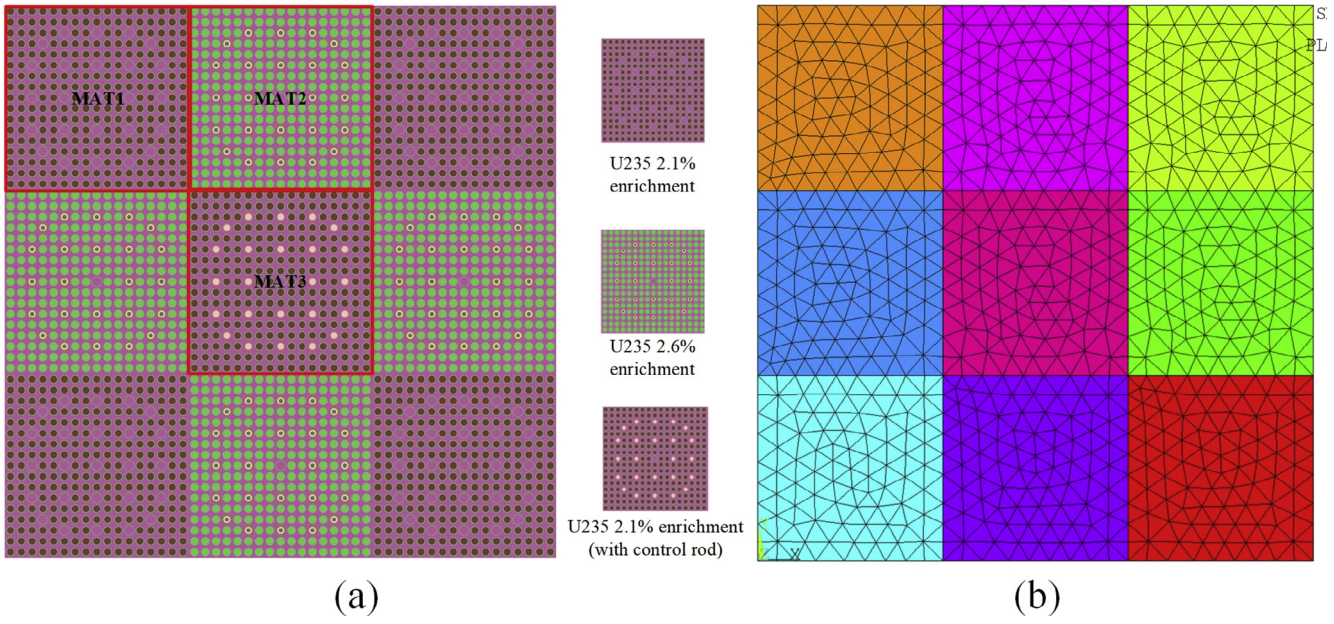


**Fig. 3.** OpenMC calculation model (a) and DNTR calculation model (b) for 2D WBN1 3 × 3 assembly benchmark. Three types of few-group homogenized cross-sections (MAT1, MAT2 and MAT3) were generated by OpenMC for DNTR transport calculation.

**Table 1**
Results for Benchmark of 2D WBN1 3 × 3 assembly at HZP and BOC.

| Case | Reference $k_{inf}$ | DNTR $k_{inf}$ | $k_{inf}$ error (pcm) | MRE of assembly power by DNTR (%) |
|---|---|---|---|---|
| WBN1-3A | 1.010238 ± 0.000013 | 1.011729 | 149.1 | 0.11 |
| WBN1-3B | 0.983446 ± 0.000012 | 0.985170 | 172.4 | 0.23 |
| WBN1-3C | 0.980291 ± 0.000013 | 0.982137 | 184.6 | 0.42 |

problem shown in Fig. 3 (a), the control rods were placed in the guide tubes of assembly with 2.1% enrichment. More details on material compositions can be referred to reference (Godfrey, 2014). 600 K was used to fuel, coolant and cladding temperatures, and thermal feedback was not considered. "Two-step" calculation scheme was performed for this benchmark: 1) three types of few-group homogenized cross-sections (Mat1, Mat2 and Mat3) were generated by OpenMC as shown in Fig. 3(a); 2) DNTR solver

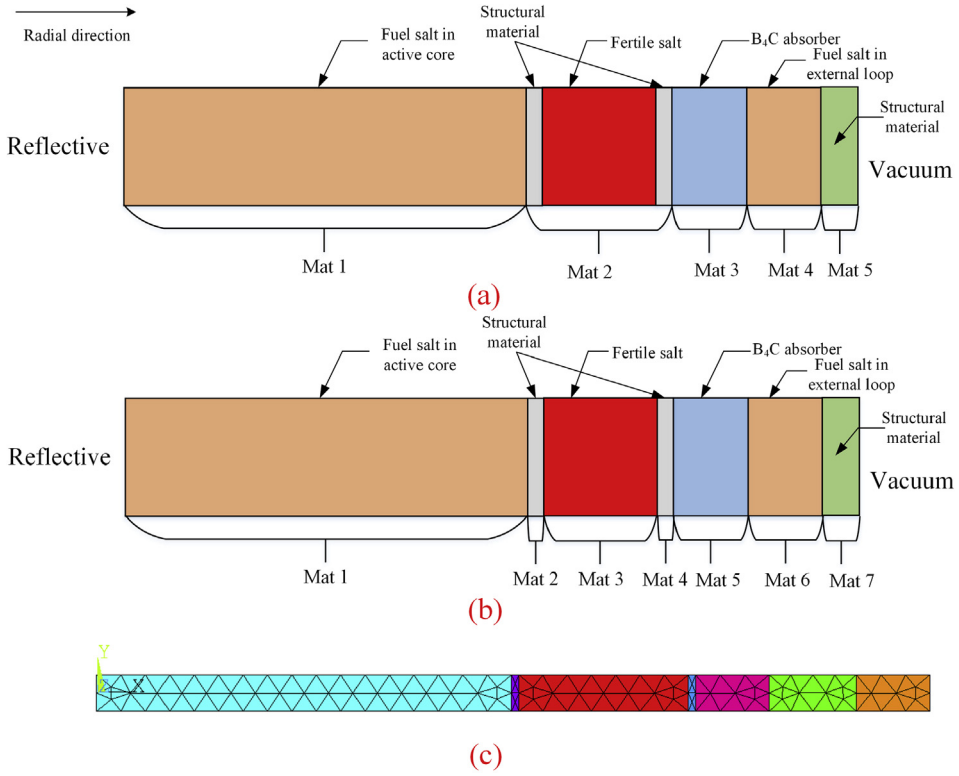


**Fig. 4.** 1D homogenization model (a), (b) for generation of few-group parameters based on MSFR radial configuration, and meshing for DNTR calculation (c).

was used for transport calculation based on those few-group cross-sections and model shown in Fig. 3(b). OpenMC calculations were performed using 100 skipped cycles, 200 active cycles and 100,0000 neutron histories per cycle. The eigenvalue $k_{inf}$, $k_{inf}$ error and the maximum relative error (MRE) of assembly power are listed in Table 1, where reference results are also presented. It can be seen that the eigenvalues by DNTR agree well with reference results, and the errors stay within 200 pcm. In addition, the MREs of assembly power are all less than 0.5% for three cases. It indicates that the few-group homogenized cross-sections generated by OpenMC are correct and can be used in whole-core calculation.

### *3.1.2. 1D homogenization model based on MSFR radial configuration*

For further verifications, two types of 1D homogenization model were built based on the reference MSFR configuration illustrated in Fig. 2. In this calculation, TRU-started case is considered, and the conclusions can be applied to U233-started case. 1D model only considers radial material arrangement of MSFR system and axial direction is infinite. 1D model has the same geometric size with MSFR radial geometry. The difference between two types of 1D model is that fertile salt and its surrounding structure material Ni-based alloy are homogenized into one homogenized material in model (a) (Mat1 to Mat5), and model (b) generated one homogenized material for each region (Mat1 to Mat7), as shown in Fig. 4.

11-group energy structure (Frima, 2013) listed in Table 2 was used for few-group homogenized cross-sections. Thermal feedback was not considered, and the uniform fuel temperature 900 K was employed for all the nuclides library in OpenMC calculations. And all the OpenMC calculations were performed using 100 skipped cycles, 200 active cycles and 1,000,000 neutron histories per cycle. Few-group cross-sections of Mat1 to Mat5 for 1D model (a) and Mat1 to Mat7 for 1D model (b) were generated, then DNTR performed transport calculations based on those cross-sections and model shown in Fig. 4(c). In DNTR calculation, model shown in Fig. 4 (c) has the same mass and volume with model shown in Fig. 4(a) or (b). The eigenvalue $k_{eff}$, relative root mean square errors (RRMSEs), flux distributions and its relative errors are summarized in Tables 3, 4 and Fig. 5, respectively, and OpenMC results serve as reference. By comparison, the $k_{eff}$ using model (b) shows a better agreement with OpenMC result than using model (a), and an error of 159.3 pcm was found for case of model (b) as shown in Table 3. As listed in Table 4, the results of DNTR with 1D model (b) have a smaller RRMSE than that of DNTR with 1D model (a) for 2nd, 4th, 6th and 8th energy group flux. As relative error of flux depicted in Fig. 5, the flux distributions calculated by DNTR with both model (a) and model (b) show a good agreement with OpenMC results in active core region. However, the flux using model (b) agree

**Table 2**
Energy group structure in MSFR simulation.

| Boundary | Neutron energy (eV) | Boundary | Neutron energy (eV) |
|---|---|---|---|
| 1 | 2.000E + 07 | 7 | 1.860E + 02 |
| 2 | 1.400E + 06 | 8 | 5.200E + 01 |
| 3 | 1.010E + 06 | 9 | 3.325E + 01 |
| 4 | 5.730E + 05 | 10 | 1.290E + 01 |
| 5 | 7.300E + 04 | 11 | 6.250E-01 |
| 6 | 2.290E + 03 | 12 | 1.000E-05 |

**Table 3**
Eigenvalue calculated by OpenMC and DNTR for 1D model.

| Case | DNTR with model (a) | DNTR with model (b) | OpenMC |
|---|---|---|---|
| Eigenvalue $k_{eff}$ | 1.082152 | 1.081613 | 1.080019 ± 3.0616E-5 |
| Error (pcm) | 213.2 | 159.3 | ~ |

**Table 4**
Relative root mean square error of 2nd, 4th, 6th and 8th energy group flux for DNTR with 1D model (a) and 1D model (b), and OpenMC results serve as reference.

| Case/Energy group | 2nd group | 4th group | 6th group | 8th group |
|---|---|---|---|---|
| DNTR with model (a) | 0.0126 | 0.0290 | 0.1363 | 1.1948 |
| DNTR with model (b) | 0.0089 | 0.0143 | 0.0210 | 0.3012 |

better with reference than flux using model (a) in other regions. Consequently, the method of using OpenMC for generation of few-group cross-sections is correct, and 1D homogenization model (b) shown in Fig. 4 can produce more accurate few-group cross-sections.

### 3.1.3. 2D homogenization model based on MSFR R-Z configuration

Fast-spectrum MSFR has longer neutron free path compared with thermal-spectrum reactor, and the local neutron spectrum will be affected by global material arrangements. Thus, the few-group cross-sections may differ as a function of space, even within the same material. To represent actual MSFR system, 2D homogenization model and DNTR calculation model were built as shown in Fig. 6, and both radial and axial influences were taken into account. The model shown in Fig. 6 (left) has the same R-Z geometric size with MSFR R-Z geometry. As with similar 1D slab model, uniform fuel temperature 900 K was employed for all the nuclides data library, and the fuel salt circulation is not considered in this calculation. As depicted in Fig. 6, 2D model is divided into 7 homogenized regions in r-direction and 4 homogenized regions in z-direction, thus, total number of 28 kinds of homogenized material need to be considered. Then, the comparison of results between DNTR and OpenMC was used to verify those few-group parameters, as shown in Table 5. Mass and volume in each homogenized region keep constant between OpenMC and DNTR calculations. An acceptable $k_{eff}$ error of 234.1 pcm is presented, and flux comparison is not plotted since it is similar with that between model (b) and OpenMC shown in Fig. 5. The results indicate the few-group cross-sections by 2D homogenized model are correct and can be used to the following whole-core calculations.

### 3.1.4. MSFR whole-core calculation by MOREL code

For few-group cross-sections generated by 1D model (b) and 2D model, the next calculation aims to verify which one is more suitable for MSFR whole-core calculation. And MOREL code developed in our previous study was adopted. MOREL is a steady and transient code for MSR analysis based on diffusion theory and ABFEN method using triangle-z node (Wang et al., 2010; Zhuang et al., 2015). The triangle nodes are generated by ANSYS-14.0 in this study, as shown in Fig. 7(a). The radial and axial nodalization of the actual MSFR core used in MOREL calculation are depicted in Fig. 7, 7 regions in radial direction and 23 layers in axial direction. Line A and Line B were plotted in Fig. 7 to show axial position when a radial neutron flux is presented and radial position when axial neutron flux is shown, respectively. Non-flowing fuel and non-thermal feedback were assumed in this calculation. The $k_{eff}$, RRMSEs, neutron flux distributions and relative errors are presented in Tables 6, 7, Figs. 8 and 9, respectively. In Fig. 9, some relative errors of flux in reflector are not plotted since OpenMC tally results are zero. As listed in Table 6, an eigenvalue error of 94.2

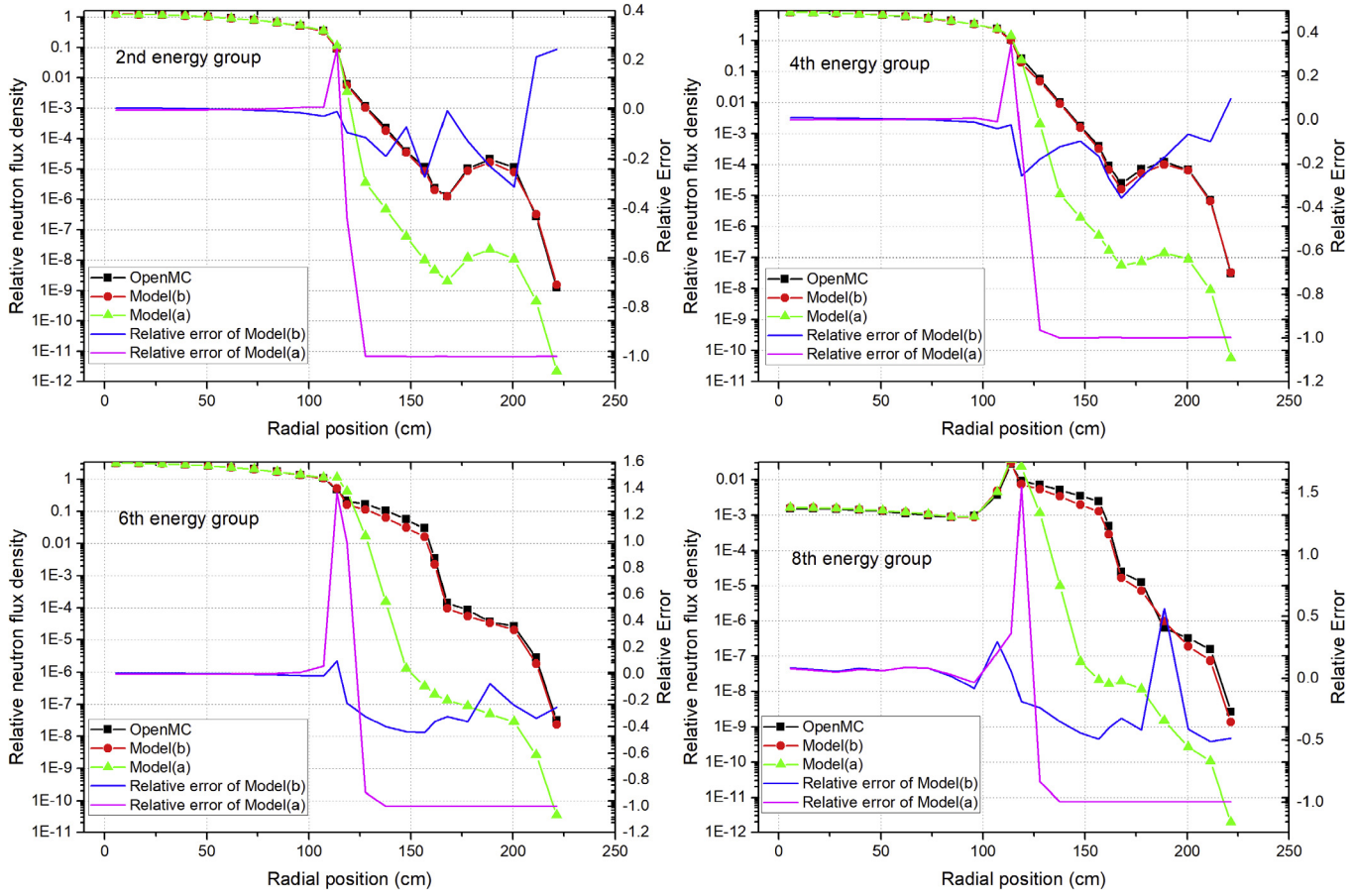


**Fig. 5.** Neutron flux radial distributions by OpenMC and by DNTR with few-group cross-sections generated by model (a) and model (b) for 1D model, and relative errors of model (a) and model (b). The flux of the 2nd, 4th, 6th and 8th energy group are selected as a comparison.

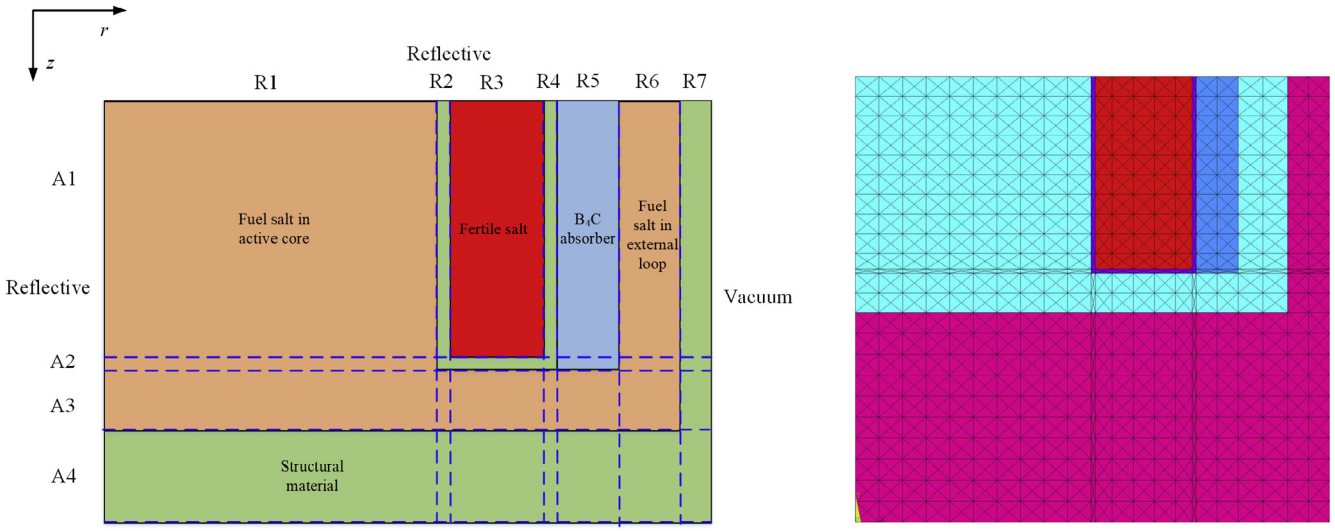


**Fig. 6.** 2D homogenization model (left-schematic not representing real geometric size) for generation of few-group parameters based on actual MSFR configuration, and meshing for DNTR calculation (right).

**Table 5**
Eigenvalue calculated by OpenMC and DNTR for 2D model.

| Code | DNTR | OpenMC | Error (pcm) |
|---|---|---|---|
| Eigenvalue $k_{eff}$ | 1.059272 | 1.056931 ± 7.1481E-5 | 234.1 |

pcm in case of using 1D model cross-sections is smaller than error of 290.1 pcm in case of using 2D model cross-sections. Compared with using cross-sections generated by 1D model (b), using cross-sections by 2D model has similar RRMSEs for radial flux distributions and smaller RRMSEs for axial flux distributions as shown in Table 7. In addition, the relative errors of both radial and axial flux distributions using 2D model cross-sections are overall smaller than that using 1D model cross-sections especially in the regions close to the reflector, as shown in Figs. 8 and 9. Consequently, the few-group cross-sections generated by 2D model are more suitable for MSFR whole-core calculation even though the few-group cross-sections generated by 1D model have better accuracy in $k_{eff}$ calculation.

**Table 6**
Eigenvalue calculated by OpenMC and MOREL for actual 3D MSFR system.

| Case | MOREL with cross-sections by 1D model | MOREL with cross-sections by 2D model | OpenMC |
|---|---|---|---|
| Eigenvalue $k_{eff}$ | 1.028672 | 1.030631 | 1.02773 ± 1.9614E-5 |
| Error (pcm) | 94.2 | 290.1 | ~ |

### 3.2. MSFR neutronics results at steady-state

In this section, some neutronics characteristics of MSFR at steady-state were calculated using MOREL code based on few-group cross-sections generated by 2D model. In this section, both U233-started case and TRU-started case with initial fuel loading are considered. THs calculation was not considered, and uniform flow field was employed for DNP calculation. Thermal feedback coefficients calculated by other institutes and MOREL code are

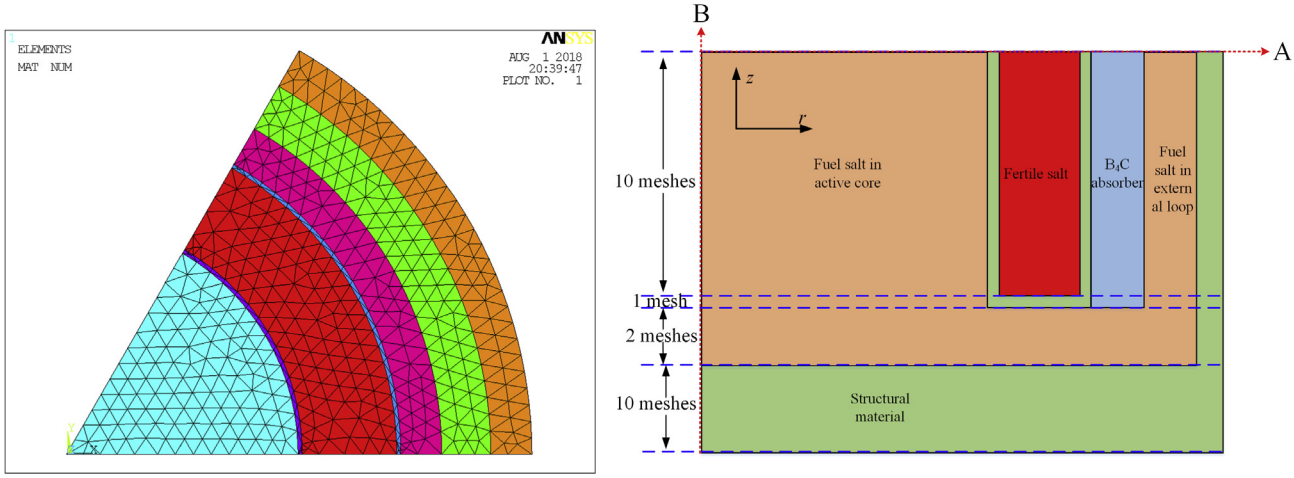


(a) MSFR whole-core radial nodalization

(b) MSFR whole-core axial nodalization

**Fig. 7.** Radial and axial nodalization for MSFR whole-core calculation.

**Table 7**
Relative root mean square of 2nd, 4th, 6th and 8th energy group flux for DNTR with cross-section by 1D model (b) and 2D model, and OpenMC results serve as reference.

| Case/Energy group | 2nd group | 4th group | 6th group | 8th group |
|---|---|---|---|---|
| DNTR with XS by X1D model (b) - radial | 0.0094 | 0.0145 | 0.0223 | 0.3253 |
| DNTR with XS by 2D model - radial | 0.0089 | 0.0130 | 0.0228 | 0.3108 |
| DNTR with XS by 1D model (b) - axial | 0.0750 | 0.0756 | 0.0797 | 1.0565 |
| DNTR with XS by 2D model - axial | 0.0079 | 0.0120 | 0.0205 | 0.2557 |

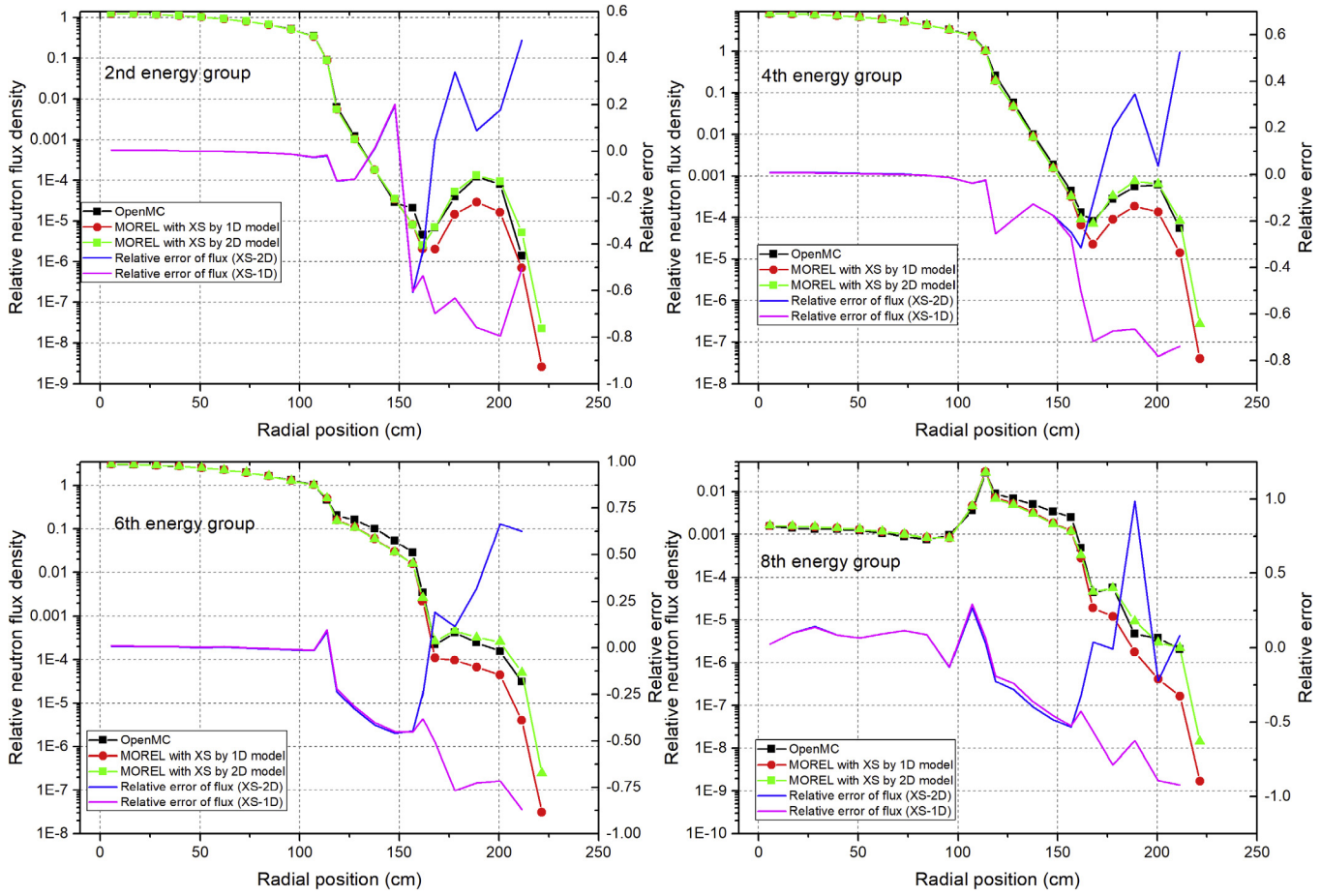


**Fig. 8.** Neutron flux radial distributions along line A by OpenMC, MOREL with few-group parameters of 1D model and 2D model for actual 3D MSFR system, and relative errors of flux with cross-sections (XS) by 1D model (b) and 2D model. The flux of the 2nd, 4th, 6th and 8th energy group are selected as a comparison.

summarized in Table 8 (Brovchenko and Merle-Lucotte, 2013). In the calculation of density coefficient, the uniform temperature of 900 K was kept for fuel salt in active core, and two cases of nuclide density at temperature of 900 K and 1000 K were performed. Thus, the density coefficient is calculated by the Equation

$$f_{density} = \frac{k_{T_2}^{density} - k_{T_1}^{density}}{\Delta T} \tag{16}$$

where $k$indicates eigenvalue; $f$ means thermal feedback coefficient; $T$represents fuel salt temperature; $\Delta T$ expresses temperature interval.

As shown in Table 8, MOREL results agree well with other institute results (KI - The Kurchatov Institute; LPSC - Laboratory of Subatomic Physics & Cosmology; POLIMI - Politecnico di Milano; POLITO - Politecnico di Torino; TU-Delft - Technical University of Delft). The density coefficient of TRU-started case is closed to that of U233-started case. However, the Doppler coefficient of U233-started case is twice larger than that of TRU-started case.

In MSFR system, the effective delayed neutron fraction is influenced by fuel salt flow field. Uniform flow field in active MSFR core was assumed in this calculation, and simulation with actual 3D flow field will be shown in the future work. The effective delayed neutron fraction with flowing ($\beta_{eff}^{flow}$) and stationary ($\beta_{eff}^{static}$) fuel are listed in Tables 9 and 10, where the definition of $\beta_{eff}^{i}$ can is shown in Eq. (17) (Mattioda et al., 2000). The calculations of $\beta_{eff}^{flow}$ and $\beta_{eff}^{static}$ are respectively based on the DNP distributions at flowing fuel and static fuel.

$$\beta_{eff}^{i} = \frac{\sum_{g=1}^{G}\int_V \varphi_g^*(r)\chi_{dgi}\lambda_i C_i(r)dv}{\sum_{g=1}^{G}\int_V \varphi_g^*(r)\chi_{dgi}\lambda_i C_i(r)dv + (1-\beta)\sum_{g=1}^{G}\sum_{g'=1}^{G}\int_V \varphi_g^*(r)\chi_{pg}\left(\nu\Sigma_f\right)_{g'}\phi_{g'}(r)dv} \tag{17}$$

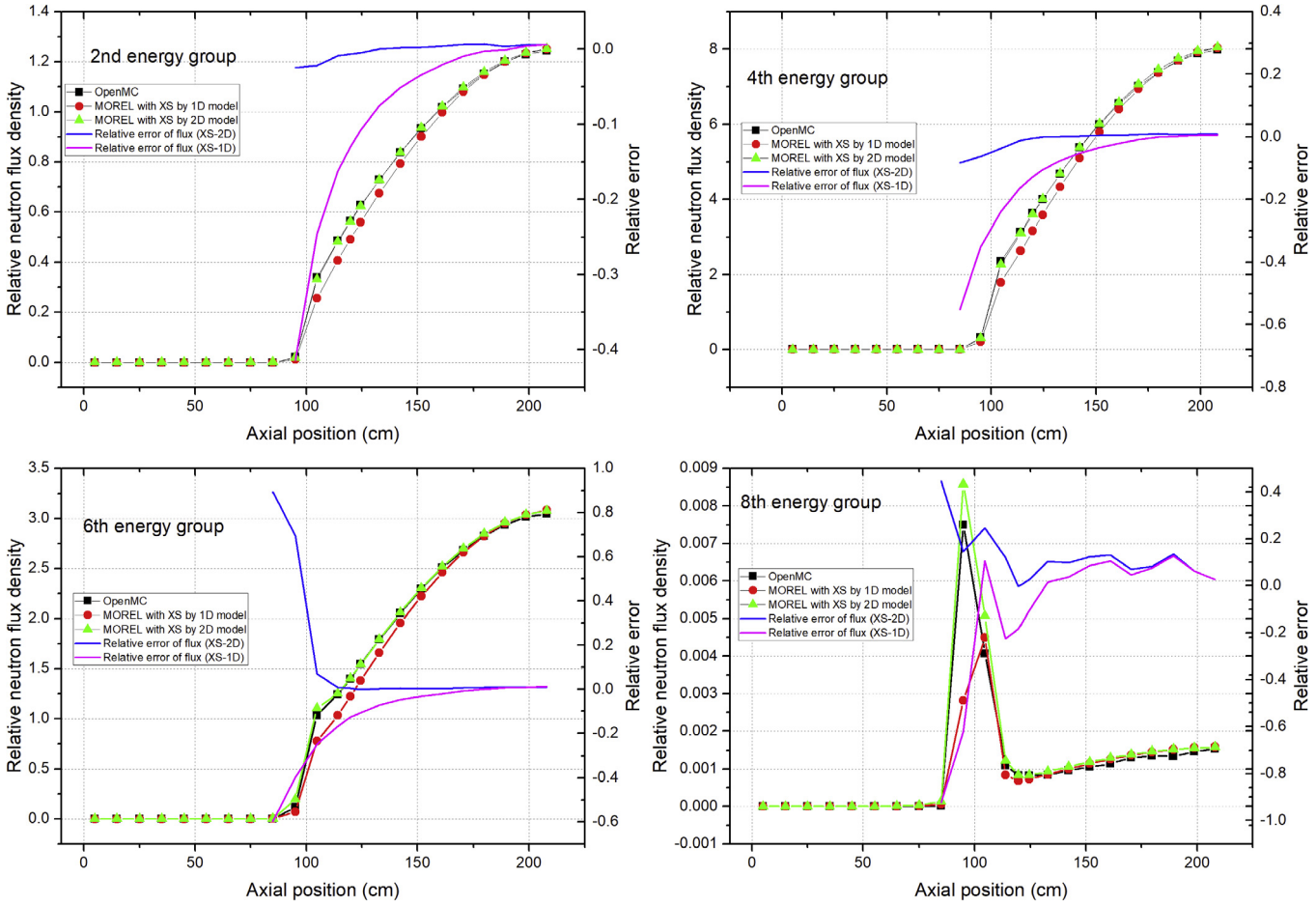


**Fig. 9.** Neutron flux axial distributions along Line B by OpenMC, MOREL with few-group parameters of 1D model (b) and 2D model for actual 3D MSFR system, and relative errors of flux with cross-sections (XS) by 1D model (b) and 2D model. The flux of the 2nd, 4th, 6th and 8th energy group are selected as a comparison.

**Table 8**
Thermal feedback reactivity coefficients of both U233-started and TRU-started case.

| Nuclides library | | KI ENDF/B-6 | LPSC ENDF/B-6 | POLIMI ENDF/B-7 | POLIMI JEFF-3.1 | POLITO JEFF-3.1 | MOREL ENDF/B-7.1 |
|---|---|---|---|---|---|---|---|
| U233-started | Doppler (pcm/K) | −4.7 | −2.6 | −3.73 | −3.84 | −3.15 | −4.01 |
| | Density (pcm/K) | −2.8 | −3.6 | −3.55 | −3.45 | −3.42 | −3.52 |
| TRU-started | Doppler (pcm/K) | −1.6 | −1.5 | −1.63 | −1.64 | −1.29 | −1.67 |
| | Density (pcm/K) | −3.4 | −2.2 | −2.75 | −2.92 | −2.85 | −2.72 |

**Table 9**
Effective delayed neutron fraction of U233-started case.

| Nuclides library | LPSC ENDF/B-6 | POLITO JEFF-3.1.1 | POLIMI JEFF-3.1 | ENDF/B-7 | TU-Delft ENDF/B-7 | MOREL ENDF/B-7.1 |
|---|---|---|---|---|---|---|
| $\beta_{eff}^{static}$(pcm) | 320.0 | 305.0 | 305.0 | 317.8 | 290.0 | 322.0 |
| $\beta_{eff}^{flow}$(pcm) | 169.46 | 117.3 | 146 | – | 124.6 | 157.4 |
| $\beta_{eff}^{loss}$(pcm) | 150.54 | 187.7 | 159 | – | 165.4 | 164.6 |

**Table 10**
Effective delayed neutron fraction of TRU-started case.

| Nuclides library | LPSC ENDF/B-6 | POLITO JEFF-3.1.1 | POLIMI JEFF-3.1 | ENDF/B-7 | MOREL ENDF/B-7.1 |
|---|---|---|---|---|---|
| $\beta_{eff}^{static}$(pcm) | 312.76 | 301.0 | 302 | 301.9 | 303.5 |
| $\beta_{eff}^{flow}$(pcm) | 165.45 | – | 147 | – | 149.3 |
| $\beta_{eff}^{loss}$(pcm) | 147.31 | – | 155 | – | 156.0 |

where subscript "static" and "flow" represent stationary and flowing fuel, respectively; The loss of effective delayed neutron fraction is defined as: $\beta_{eff}^{loss} = \beta_{eff}^{static} - \beta_{eff}^{flow}$.

where $V$ is all computational space; $\varphi^*$ is adjoint flux; The total effective delayed neutron fraction is defined as $\beta_{eff} = \sum_{i=1}^{I} \beta_{eff}^{i}$; $I$ is the total family group of DNPs; other notations have the same meaning with that in Eqs. (7-11).

It can be seen that MOREL results and other researchers are in a good agreement, and the effective delayed neutron fraction of TRU-started case is slightly smaller than U233-started case for all researchers. Due to the equal residence time of fuel salt in reactor core and in external loop, $\beta_{eff}^{loss}$ is nearly equal to $\beta_{eff}^{flow}$ both for U233-started and TRU-started case.

## 4. Conclusion

The MSFR system is featured by fast-spectrum and has a longer neutron free path compared to thermal-spectrum reactor. Therefore, lattice code prepared for thermal-spectrum reactor is not suitable for MSFR calculation. This study developed a tool TRANS to transfer tally data from an open source Monte Carlo code OpenMC into few-group homogenized cross-sections, and the verification of TRANS was performed with one PWR benchmark and two types of model based on MSFR. Besides, the applicability of few-group parameters generated by different model for MSFR whole-core calculation was also analyzed. Finally, MSFR neutronics characteristics at steady-state were calculated using MOREL. The main conclusions are listed below.

(1) In benchmark of WBN1 $3 \times 3$ assembly, and 1D and 2D MSFR model, the few-group parameters generated by OpenMC are correct. Consequently, the method using OpenMC to generate few-group parameters is feasible.
(2) In case of 1D homogenization model, few-group parameters by 1D model (b) can give more accurate results both for eigenvalue and flux distribution.
(3) In MSFR whole-core calculation, using few-group cross-sections generated by 2D model has better accuracy in flux distribution, however, using few-group cross-sections generated by 1D model has better accuracy in $k_{eff}$ calculation.
(4) The neutronics parameters of MSFR calculated by MOREL code agree well with that by other institutes.

## Acknowledgements

Thank Computational Reactor Physics Group at MIT for providing open source Monte Carlo code OpenMC. Thank Nuclear Engineering Computational Physics Lab. (NECP) at Xi'an Jiaotong University for providing DNTR transport solver. This work was supported by the Fundamental Research Funds for the Central Universities under Grant YAH17067.

## References

Allibert, M., Aufiero, M., Brovchenko, M., Delpech, S., Ghetta, V., Heuer, D., Laureau, A., Merle-Lucotte, E., 2016. Molten salt fast reactors. Woodhead Publishing, Cambridge (UK).
Aufiero, M., Brovchenko, M., Cammi, A., 2014. Calculating the effective delayed neutron fraction in the molten salt reactor: analytical, deterministic and Monte Carlo approches. Ann. Nucl. Energy. 65, 78–90.
Aufiero, M., Cammi, A., Fiorina, C., Leppänen, J., Luzzi, L., Ricotti, M.E., 2013. An extended version of the SERPENT-2 code to investigate fuel burn-up and core material evolution of the Molten Salt Fast Reactor. J. Nucl. Mater. 441, 473–486.
Bettis, E.S., Schroeder, R.W., Cristy, G.A., 1957. The aircraft reactor experiment—design and construction. Nucl. Sci. Eng. 2, 804–825.
Briesmeister, J.F., 1997. MCNP4B – A general Monte Carlo N Particle Transport Code. LA-12625-M, Los Alamos Laboratory, Los Alamos, NM, USA.
Brovchenko, M., Merle-Lucotte, E., 2013. Optimization of the pre-conceptual design of the. MSFR - EVOL, project.
Fiorina, C., Aufiero, M., Cammi, A., Franceschini, F., Krepel, J., Luzzi, L., Mikityuk, K., Ricotti, M.E., 2013. Investigation of the MSFR core physics and fuel cycle characteristics. Prog. Nucl. Energ 68, 153–168.
Fiorina, C., Lathouwers, D., Aufiero, M., Cammi, A., Guerrieri, C., Kloosterman, J.L., Luzzi, L., Ricotti, M.E., 2014. Modelling and analysis of the MSFR transient behaviour. Ann. Nucl. Energy. 64, 485–498.
Fridman, E., Leppänen, J., 2011. On the use of the Serpent Monte Carlo code for few-group cross section generation. Ann. Nucl. Energy. 38, 1399–1405.
Frima, L.L.W., 2013. Burnup in a Molten Salt Fast Reactor, Department of Radiation Science and Technology. Delft University of Technology, Delft, The Netherlands.
Godfrey, A.T., 2014. VERA Core Physics Benchmark Progression Problem Specifications. CASL-U-2012-0131-004. Oak Ridge National Laboratory.
Haubenreich, P.N., 1969. Molten salt reactor experiments. United States.
Heuer, D., Merle-Lucotte, E., Allibert, M., Brovchenko, M., Ghetta, V., Rubiolo, P., 2014. Towards the thorium fuel cycle with molten salt fast reactors. Ann. Nucl. Energy. 64, 421–429.
Hu, T., Cao, L., Wu, H., Du, X., He, M., 2017. Coupled neutronics and thermal-hydraulics simulation of molten salt reactors based on OpenMC/TANSY. Ann. Nucl. Energy. 109, 260–276.
Leppänen, J., Pusa, M., Viitanen, T., Valtavirta, V., Kaltiaisenaho, T., 2015. The Serpent Monte Carlo code: status, development and applications in 2013. Ann. Nucl. Energy. 82, 142–150.
Li, Y., 2012. Advanced Reactor Core Neutronics computational algorithms based on the variational nodal and nodal SP3 methods. Jiaotong University, Xi'an(China).
Li, Z., Cao, L., Wu, H., He, Q., 2016. The impacts of thermal neutron scattering effect and resonance elastic scattering effect on FHRs. Ann. Nucl. Energy. 97, 102–114.
Linden, E.v.d., 2012. Coupled neutronics and computational fluid dynamics for the molten salt fast reactor. Delft University of Technology, Delft.
Lu, H., Wu, H., 2007. A nodal SN transport method for three-dimensional triangular-z geometry. Nucl. Eng. Des. 237, 830–839.
MacFarlane, R.E., Muir, D.W., 1994. The NJOY nuclear data processing system, Version 91. USA LA-12740-M, Los Alamos, NM.
Mattioda, F., Ravetto, P., Ritter, G., 2000. Effective delayed neutron fraction for fluid-fuel systems. Ann. Nucl. Energy. 27, 1523–1532.
Merle-Lucotte, E., Heuer, D., Allibert, M., Brovchenko, M., Capellan, N., Ghetta, V., 2011. Launching the thorium fuel cycle with the Molten Salt Fast Reactor. In: 2011 International Congress on Advances in Nuclear Power Plants (ICAPP 2011), Nice, France, pp. 842–851.
Nuttin, A., Heuer, D., Billebaud, A., Brissot, R., Le Brun, C., Liatard, E., Loiseaux, J.M., Mathieu, L., Meplan, O., Merle-Lucotte, E., Nifenecker, H., Perdu, F., David, S., 2005. Potential of thorium molten salt reactors: detailed calculations and concept evolution with a view to large scale energy production. Prog. Nucl. Energ. 46, 77–99.
Pioro, I.L., 2016. Introduction: generation IV international forum. Woodhead Publishing, Cambridge (UK).
Powers, J.J., Harrison, T.J., Gehin, J.C., 2013. A new approach for modeling and analysis of molten salt reactors using SCALE, M&C 2013: International Conference on Mathematics and Computational Methods Applied to Nuclear Science and Engineering. Sun Valley, ID, USA.
Rachamin, R., Wemple, C., Fridman, E., 2013. Neutronic analysis of SFR core with HELIOS-2, Serpent, and DYN3D codes. Ann. Nucl. Energy. 55, 194–204.
Romano, P.K., Horelik, N.E., Herman, B.R., Nelson, A.G., Forget, B., Smith, K., 2015. OpenMC: a state-of-the-art Monte Carlo code for research and development. Ann. Nucl. Energy. 82, 90–97.
Rosenthal, M.W., Haubenreich, P.N., Briggs, R.B., 1972. Development status of Molten-Salt Breeder Reactors. ORNL–4812, United States.
Serp, J., Allibert, M., Beneš, O., Delpech, S., Feynberg, O., Ghetta, V., Heuer, D., Holcomb, D., Ignatiev, V., Kloosterman, J.L., Luzzi, L., Merle-Lucotte, E., Uhlíř, J., Yoshioka, R., Zhimin, D., 2014. The molten salt reactor (MSR) in generation IV: Overview and perspectives. Prog. Nucl. Energ. 77, 308–319.
Sheu, R.J., Chang, C.H., Chao, C.C., Liu, Y.-W.H., 2013. Depletion analysis on long-term operation of the conceptual Molten Salt Actinide Recycler & Transmuter (MOSART) by using a special sequence based on SCALE6/TRITON. Ann. Nucl. Energy. 53, 1–8.
Tuominen, R., 2015. Coupling Serpent and OpenFOAM for neutronics – CFD multi-physics calculations. Aalto University, Aalto.
Wang, J., Cao, X., 2016. Investigation on fluctuations in full-size Molten Salt Reactor with coupled neutronic/thermal-hydraulic model. Ann. Nucl. Energy. 92, 262–276.
Wang, K., Wu, H., Cao, L., Wang, C., 2010. Analytic Basis Function Expansion Nodal Method for Neutron Diffusion Equations in Triangular Geometry. 151–157.
Yang, W.S., 2012. Fast reactor physics and computational methods. Nucl. Eng. Technol. 42, 117–198.
Yu, C., Li, X., Cai, X., Zou, C., Ma, Y., Wu, J., Han, J., Chen, J., 2017. Minor actinide incineration and Th-U breeding in a small FLiNaK Molten Salt Fast Reactor. Ann. Nucl. Energy. 99, 335–344.
Zhang, D.L., Qiu, S.Z., Su, G.H., Liu, C.L., Qian, L.B., 2009. Analysis on the neutron kinetics for a molten salt reactor. Prog. Nucl. Energ. 51, 624–636.
Zhou, S., 2017. Neutronics calculation and fuel cycle analysis of accelerator driven subcritical transmuters. Xi'an Jiaotong University.
Zhou, S., Yang, W.S., Park, T., Wu, H., 2018. Fuel cycle analysis of molten salt reactors based on coupled neutronics and thermal-hydraulics calculations. Ann. Nucl. Energy. 114, 369–383.
Zhuang, K., Cao, L., Zheng, Y., Wu, H., 2015. Studies on the molten salt reactor Code development and neutronics analysis of MSRE-type design. J. Nucl. Sci. Technol. 52, 251–263.
Zhuang, K., Zheng, Y., Cao, L., Hu, T., Wu, H., 2017. Improvements and validation of the transient analysis code MOREL for molten salt reactors. J. Nucl. Sci. Technol. 54, 878–890.